Proceedings of ASME Turbo Expo 2011
GT2011
June 6-10, 2011, Vancouver, British Columbia, Canada

GT2011-46006

A COMPARATIVE STUDY OF CASCADE VANES AND DRILLED NOZZLE DESIGNS FOR PRE-SWIRL

Umesh Javiya
u.javiya@surrey.ac.uk

John Chew
j.chew@surrey.ac.uk

Nick Hills
n.hills@surrey.ac.uk

Thermo-Fluid Systems
Faculty of Engineering and Physical Science
University of Surrey
Guildford, Surrey, GU2 7XH, UK

Timothy Scanlon
PO Box 31,
Rolls-Royce Plc, Derby, UK

ABSTRACT

Design of pre-swirl systems is important for the secondary air cooling system of gas turbine engines. In this paper, three pre-swirl nozzles, a cascade vane and two drilled nozzles are analysed and their performances are compared. The two drilled nozzles considered are a straight drilled nozzle and an aerodynamically designed nozzle. CFD analyses are presented for stand-alone and pre-swirl system 3D sector models at engine operating conditions near to engine maximum power condition rotational Reynolds number (Re_ϕ) up to 4.6 ! 10^7. Nozzle performance is characterised by the nozzle discharge coefficient (C_D), nozzle velocity coefficient (η) and cooling air delivery temperature. Two commonly used eddy viscosity models are employed for the study, the standard *k-ε* and Spalart-Allmaras models with wall functions. Both models give very similar results for C_D and η, and are in reasonable agreement with available experimental data. Effects of nozzle or vane number and sealing flow have been analysed. The cascade vanes perform slightly better than the aerodynamically designed drilled nozzles but the final design choice will depend on other component and manufacturing costs. An elementary model is presented to separate temperature losses due to the nozzle, stator drag and sealing flow.

NOMENCLATURE

A	area, m^2
A_N	nozzle throat area, m^2
c	friction factor
C_D	discharge coefficient
C_p	specific heat capacity at constant pressure, J/kg K
C_w	non-dimensional mass flow rate ($\dot{m}/\mu r_h$)
D	moment on the stator walls, Nm
d_p	nozzle down stream diameter, m
k	turbulence kinetic energy, m^2/s^2
l	cascade vane's chord length, m
$\dot{m}$	mass flow rate, kg/s
M	moment on the rotor walls, Nm
N_p	number of pre-swirl nozzles
p	static pressure, N/m^2
P	absolute total pressure, N/m^2
Q	heat transfer to the system, W
r	radius, m
r_h	receiver hole radial location, m
r_p	nozzle exit radial location, m
Re_ϕ	rotational Reynolds number, ($\rho\Omega r_h^2/\mu$)
SR	swirl fraction, ($v_\phi/\Omega r$)
t_p	pre-swirl plate thickness, m
T	absolute total temperature, K
T_{rel}	total temperature in rotating reference frame, K
u_τ	friction velocity, m/s
V	velocity magnitude, m/s
v_ϕ	swirl/tangential velocity, m/s

y	distance normal to the wall, m
y^+	non-dimensional wall distance ($\rho y u_\tau/\mu$)
α	drilled nozzle chamfer angle
ε	turbulence dissipation rate, m^2/s^3
ρ	density of air, kg/m^3
μ	dynamic viscosity of air, Ns/m^2
Ω	rotation speed of the rotor disc, rad/s
η	velocity coefficient of the nozzle
θ	nozzle angle to the tangential direction, degree
γ	ratio of specific heats

Subscript

dim	non-dimensional
h	at receiver hole
in	At nozzle or vanes inlet
isen	isentropic
mix	for mixed condition
p	at pre-swirl nozzle exit
r	at radial location *r*
rel	relative to rotating reference frame
rotor	for rotor
s	at inner seal
stator	for stator
ϕ,*z*	circumferential and axial coordinates

1 INTRODUCTION

In modern gas turbine engines cooling air is drawn from a compressor stage giving the appropriate level of pressure for the secondary air system. The use of this air incurs a thermal efficiency penalty as it is removal from the main flow path and does not contribute for direct thrust or power. The secondary air is used to cool the turbine disc components and suppress hot gas ingestion into the turbine cavities. In a high-pressure turbine stage, this cooling air is expanded through stationary, angled pre-swirl nozzles or vanes, transferred through a wheel-space, and delivered to blade receiver holes on the rotating disc. The nozzles swirl the air in the direction of the rotor rotation. This reduces the work done by the rotating turbine disc in accelerating the air to the disc speed, and reduces the relative total temperature of the air supplied to the rotor-blade roots (compare to that without pre-swirl).

The cooling air delivery temperature for an ideal pre-swirl chamber without sealing flow or windage effects can be given by the following equation.

$$T_{rel,h} = T_{in} - \frac{\Omega^2 r_h^2}{2C_p}\left\{2\left(\frac{r_p}{r_h}\right)^2 \cdot \eta \cdot SR_{isen,p} - 1\right\} \qquad (1)$$

where, η is nozzle velocity coefficient and $SR_{isen,p}$ is isentropic swirl ratio at the nozzle exit. η and $SR_{isen,p}$ are given by the following expressions.

$$\eta = \frac{v_{\phi,p}}{v_{\phi,isen,p}} \qquad and \qquad SR_{isen,p} = \frac{v_{\phi,isen,p}}{\Omega r_p} \qquad (2)$$

In the above T_{in} is the total temperature at the nozzle inlet in the absolute reference frame. $T_{rel,h}$ is total temperature at the receiver holes outlet in the rotating reference frame, which is referred to here as the cooling air delivery temperature of the pre-swirl system. $T_{rel,h}$ is particular significant it is the available relative total temperature for the turbine blade cooling. r_p and r_h are radial locations of the nozzle exit and receiver holes respectively. Ω is rotational speed of the rotor and C_p is constant pressure specific heat. $v_{\phi,isen,p}$ is isentropic swirl velocity at the nozzle exit. In reality the nozzle velocity coefficient, η is always less than the ideal value of 1. The η value can be improved by better design of the nozzle. The above simple relation indicates that a 5% improvement in η could lead to an improvement of ~10% in delivery cooling air temperature difference (T_{in} - $T_{rel,h}$) (for r_p~ r_h and $SR_{isen,p}$= 1). This emphasizes the importance of the nozzle design in the pre-swirl system.

A number of experimental and numerical studies have been carried out to understand flow and heat transfer processes in pre-swirl systems. Examples are given in references [1 to 9]. Meierhofer and Franklin [1] were the first to publish an experimental investigation on a pre-swirl system. They used cascade vanes to generate pre-swirl and characterised pre-swirl effectiveness by an equivalent velocity coefficient (η) for the nozzle. The results indicated that the effectiveness is not affected significantly by different arrangement of the nozzles and pre-swirl chamber width. Other researchers have used drilled nozzles to generate pre-swirl flow. See, for example, Chew et al. [10], Bricaud et al. [11] and Dittmann et al. [12]. Using computational fluid dynamics (CFD) as an optimisation tool, Ciampoli et al. [13] have looked at drilled nozzle design. They showed notable improvements in velocity coefficient could be achieved by careful aerodynamic design of the nozzle.

Several studies have been carried out for discharge behaviour of nozzle and orifices. Reviews of cooling hole discharge coefficients can be found in Hay and Lampard [14] and McGreehan and Schotsch [15]. Recently Chew et al. [10], Bricaud et al. [11] and Dittmann et al. [12] have published experimental measurements for discharge coefficients for the drilled pre-swirl nozzles. According to these studies, the discharge behaviour of the nozzles depends on the nozzle design and nozzle Reynolds number, but only weakly depends on the number of nozzles, pre-swirl chamber size and arrangement of the nozzles.

In this paper different design approaches for the pre-swirl nozzles are compared using steady state CFD analysis. Three nozzle designs, simple straight drillings, aerodynamically shaped drillings and cascade vanes are considered. Analyses are presented for standalone nozzles as well as for a full pre-swirl system near to engine maximum power conditions. The effects of varying numbers of nozzles or vanes on the delivery cooling air temperature and the effects of sealing flow on the pre-swirl performance for both nozzles are also presented.

In the next section details of the nozzle designs and model are given. A description of the CFD modelling approach follows in section 3. The nozzle performances in terms of discharge and velocity coefficients are compared in section 4.1 and 4.2 respectively. The results for the cooling air delivery temperature and effect of different numbers of nozzles are presented in section 4.3. An elementary analysis of system behaviour is compared with CFD results in section 5 and overall conclusions are given in section 6.

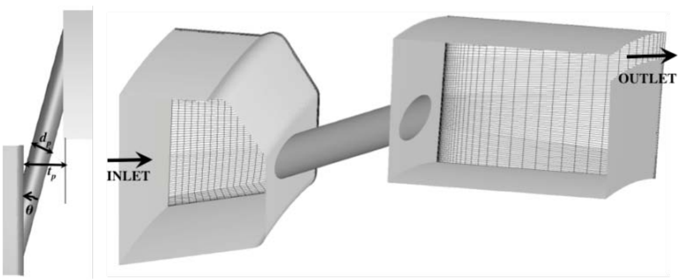

(a) Simple drilled (SD) nozzle

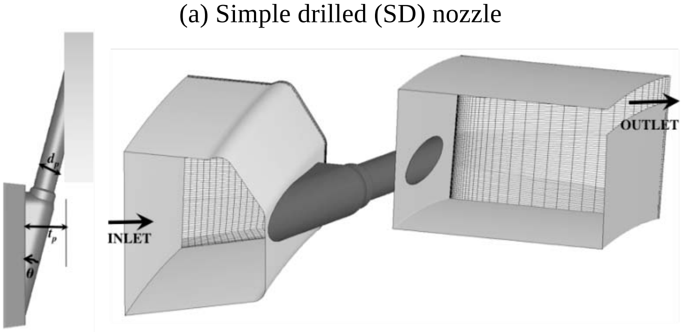

(b) Aerodynamically shaped drilled (AD) nozzle

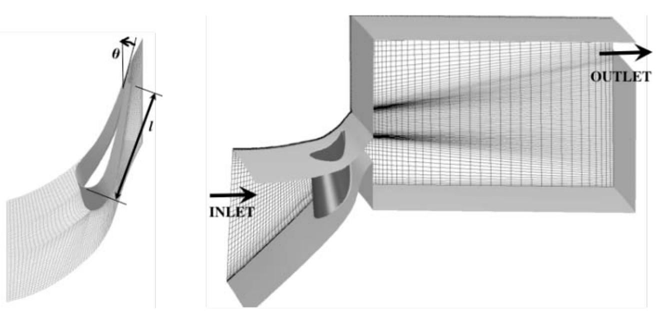

(c) Cascade vane (VANES)

Figure 1: Standalone nozzle models

2 NOZZLE DESIGNS

The nozzle designs are shown in Figure 1. To simplify discussion, the simple straight-drilled nozzle, aerodynamically shaped nozzle and cascade vanes will be referred as SD, AD and VANES respectively throughout the discussion. Some geometric features of the nozzles are given in Table 1. The SD nozzle has a diameter of 7.2 mm. The AD nozzle design considered here is similar to Ciampoli et al.'s [13] optimised nozzle design, and has the same downstream diameter as the SD nozzle. The opening throat area (A_N) of the VANES is very similar to the drilled nozzles. The mid-radial location of the nozzle or vane exit (r_p) is the same for all three nozzles. All three nozzles are angled at the same angle (θ =15 degree) in the same direction of the turbine disc rotation.

2.1 Standalone nozzle models

The standalone nozzle analysis were performed with plena at the nozzle entry and exit. Periodic sectors corresponding to one nozzle models are shown in Figure 1. The plenum at the exit is created in the same way as by Javiya et al. [9], with an axisymmetric slot for the outlet at a higher radius to avoid any reverse flow at the outlet boundary. Dimensions of the exit plenum are approximately the same for all nozzles, hence it was assumed that the exit plenum provides very similar back pressures resistance at nozzle exit. The insensitivity of results to the exit plenum size was confirmed by increasing plenum size by a factor of two for the cascade vanes model in one test case. The results for discharge coefficient and nozzle velocity coefficient for different plenum size are given in section 3.

Parameters	Description	Cascade vanes	Drilled nozzles
N_p	Number of nozzles/vanes	96	38
t_p (mm)	Pre-swirl plate thickness	-	13.0
d_p (mm)	Downstream nozzle diameter	-	7.2
l (mm)	Chord length	20.25	-
α	Chamfer angle		45^o
θ	Exit angle to circumferential direction	15^o	15^o
r_p/r_h	Ratio of radial locations of nozzle exit to receiver hole inlet	0.9416	0.9416

Table 1: Geometry data for the nozzles

2.2 System models

For the pre-swirl system analyses the nozzles were attached to a pre-swirl chamber very similar to that considered by Snowsill and Young [16]. The receiver holes were modelled as an axisymmetric slot with the same total area as the holes to allow steady state simulations. The periodic sector model for the VANES nozzle is shown in Figure 2. In practice significant sealing flow enters through the inner seal, which is usually at a higher temperature than the main pre-swirl flow (Snowsill and Young [16]). There is also a leakage through the outer seal from the pre-swirl chamber seal as shown in Figure 2. A similar periodic sector system model was created with the AD nozzle. In the system analysis, the sealing flow was modelled by providing an inlet and outlet as illustrate in Figure 2. In this figure rotating walls are coloured red and all other walls are stationary.

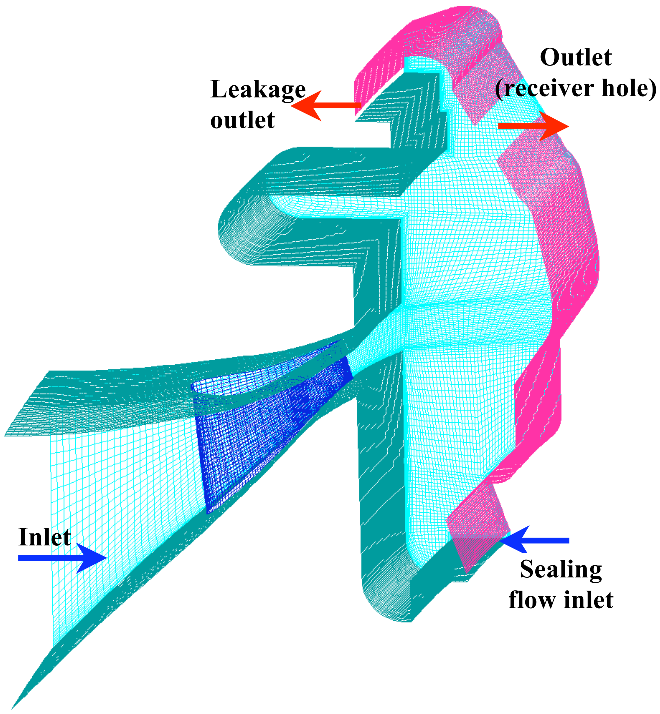

Figure 2: Pre-swirl system model with the VANES nozzle

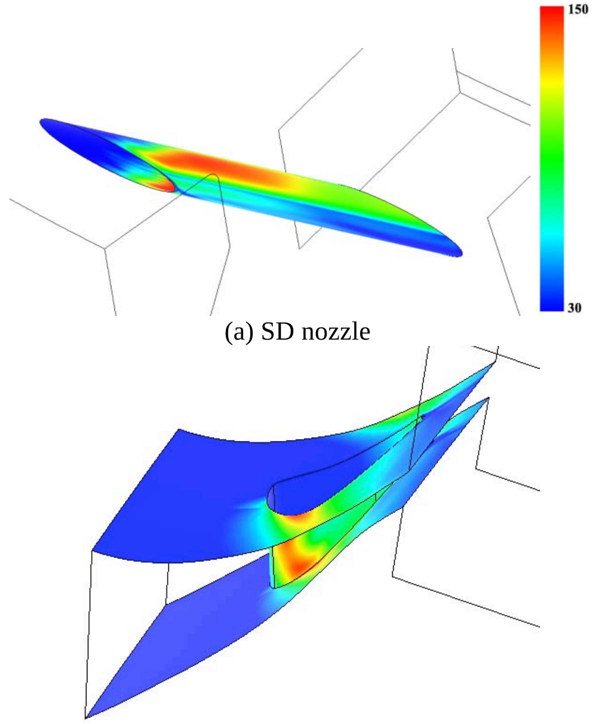

(a) SD nozzle

(b) VANES nozzle

Figure 3: y+ values

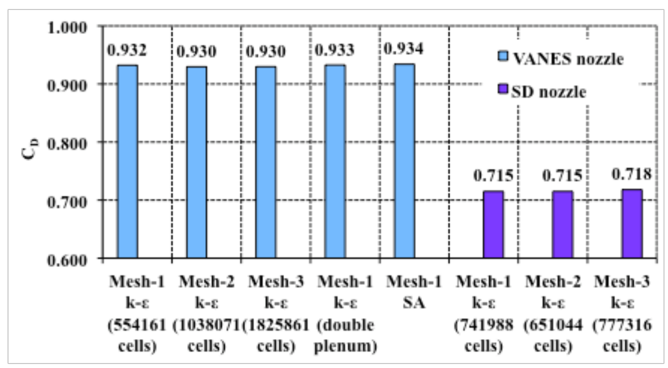

Figure 4: Mesh dependency study

3 CFD MODELLING

All CFD simulations were carried out as steady state with second order discretisation accuracy with the Hydra CFD solver [17]. Hydra is a suite of linear, non-linear and adjoint solvers, developed by Rolls-Royce and its partner universities. In this work, a density based non-linear steady state solver [18] was used. This uses block Jacobi precondition and the 5 stage Runga-Kutta scheme of Martinelli [19]. Convergence acceleration was achieved with an edge collapsing based multigrid algorithm [20]. Hydra uses Oplus (Oxford Parallel libraries for unstructured Solvers) libraries for parallel computations as described by Hills [21].

In all simulations walls are specified as adiabatic, no-slip boundaries. Constant total pressure or mass flow rate at inlets and constant static pressure at the outlet boundaries were specified. For the stand alone nozzle analysis, two different turbulence models, Spalart-Allmaras (SA) [22] and standard k-ε with wall functions, were tested.

Several meshes have been created with different mesh density in radial, axial and circumferential directions, but keeping the range of 30 to 150 over most of the nozzle walls. The y+ values for one of the meshes are shown in Figure 3 for the SD and VANES nozzles with the k-ε turbulence model. Similar range of y+ values was kept for the AD nozzles. Near to the stagnation region of the nozzle inlets y+ values are below 30 because of very low velocities. Hence, the results presented here may be subject to these limitations.

For the mesh dependency study, nozzle discharge coefficients (C_D) were compared. Results for the SD and VANES nozzle on three meshes are shown in Figure 4. The mesh sizes and calculated C_D values with three different meshes are given in Figure 4. The C_D values were calculated using the following equation [10],

$$C_D = \frac{\dot{m}_p}{A_N \dfrac{P_{in}}{RT_{in}} \left(\dfrac{p_p}{P_{in}} \right)^{1/\gamma} \cdot V_{isen,p}} \tag{3}$$

where, $\dot{m}_p$ is calculated mass flow rate through the nozzle, A_N is nozzle throat area. $V_{isen,p}$ is isentropic velocity at nozzle exit, given by,

$$V_{isen,p} = \left[2C_p T_{in} \left(1 - \left(\frac{p_p}{P_{in}} \right)^{\frac{\gamma-1}{\gamma}} \right) \right]^{0.5} \tag{4}$$

where, P_{in} and T_{in} correspond to the inlet boundary condition and p_p was taken as the area weighted average value at the nozzle exit.

As shown in Figure 4 the calculated C_D values are varied within 0.3% of the mesh-1 C_D value.. Hence the results presented here could be considered as mesh independent. Further results are presented with mesh-1 for SD and VANES nozzles. The mesh density in the AD nozzles was kept the same as for the SD nozzles. Figure 4 also shows the calculated C_D with the double size plenum at outlet for the vanes nozzle. Again the C_D values are within 0.3% of the mesh-1 C_D value. In Figure 4, the results are shown for two different turbulence models for mesh-1 for the VANES nozzle. The results showed insensitivity to choice of turbulence model, and so only the k-ε turbulence model was used for further studies.

4 RESULTS

To compare nozzle performance, C_D and η values were calculated for the stand alone as well as the full pre-swirl system analysis. The cooling air delivery temperatures are compared in the full pre-swirl system analysis only.

4.1 Nozzle performance

For validation of CFD calculations, the calculated C_D values for stand-alone nozzle models are compared with Chew et al.'s [10] experimental data for pre-swirl drilled nozzle data. Chew et al.'s drilled nozzles were aerodynamically designed but are not exactly the same as the AD nozzles considered here. Chew et al.'s nozzle had higher θ = 20 degree and longer chamfer length than the AD nozzle considered here. The calculated and measured C_D values are plotted against pressure ratio in Figure 5. Calculated C_D values for AD and VANES nozzles are within the range of the measurements. Differences could be explained by different design and Reynolds number effects. For the experiments a representative nozzle exit Reynolds number ($=\rho V d_p/\mu$) was estimated as 1.83×10^5 for a pressure ratio of 1.524. In the calculations, the nozzle Reynolds number is 1.33×10^6 at this pressure ratio. The C_D values are significantly higher for aerodynamically designed AD and VANES nozzles than SD nozzles. The C_D values for the SD nozzle are in the range expected for long orifices as presented, for example, by McGreehan and Schotsch [15].

Calculated velocity coefficients (η) are shown in Figure 6 for stand alone and pre-swirl system models. As for the C_D values, the η values are higher for aerodynamically designed nozzles than SD nozzles. The VANES nozzles give the highest ηvalues, hence the VANES nozzles are expected to perform better in the full pre-swirl system analysis. The η values are very similar for stand alone and system models. This confirms that the presence of the rotor disc does not significantly affect results, as is consistent with Bricaud et al.'s [11] and Dittmann et. al's [12] experimental data. The plot also shows η values with the number of the AD nozzles reduced by half to 19 but keeping the same total nozzle area and the number of VANES reduced by a third to 64 by closing every third vane. The η values are not sensitive to these changes. Hence, it is concluded that changing the arrangement of nozzles does not significantly affect the discharge behaviour of the nozzle for the operating conditions simulated here.

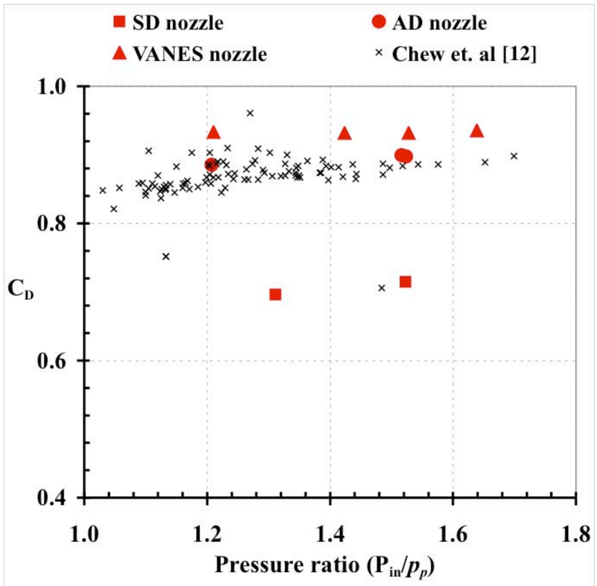

Figure 5: Discharge coefficient (C_D) versus pressure ratio across the nozzles

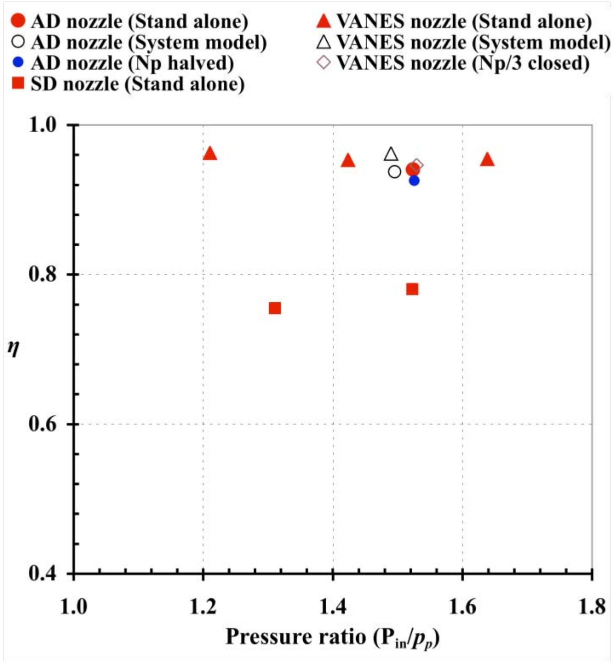

Figure 6: Velocity coefficient (η) versus pressure ratio across the nozzles

4.2 Delivery cooling air temperature

Calculated non-dimensional temperature drop (ΔT_{dim}) versus isentropic inlet swirl ratio ($SR_{isen,p}$) is shown in Figure 7 for the full pre-swirl system analysis. The graph shows results for non-dimensional flow conditions, $Re_\phi = 3.93 \times 10^7$ to 4.58×10^7 and $C_w = 4.21 \times 10^5$ to 6.31×10^5 with and without sealing flow. ΔT_{dim} is calculated using the following equation [4],

$$\Delta T_{\text{dim}} = \frac{C_p\left(T_{in} - T_{rel,h}\right)}{0.5\Omega^2 r_h^2} \tag{4}$$

where, T_{in} is absolute total temperature at nozzle inlet and $T_{rel,h}$ is total temperature in the rotating reference frame at receiver hole. Re_ϕ and C_w were calculated based on the nozzle inlet conditions.

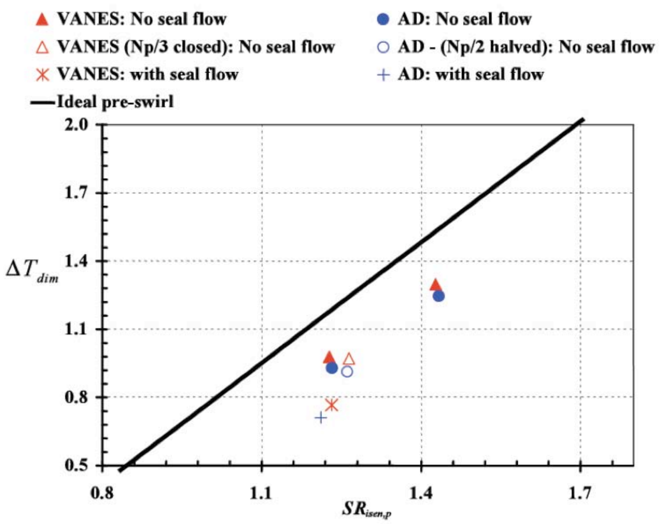

Figure 7: ΔT_{dim} versus $SR_{isen,p}$ for pre-swirl system models

Figure 7 also shows the ideal pre-swirl performance with a thick black line (η= 1in equation (1)). The difference between the ideal pre-swirl curve and calculated ΔT_{dim} is due to losses in the nozzle, wall drag inside the pre-swirl chamber and sealing flow. It can be seen that the VANES nozzles give a slightly higher temperature drop than the AD nozzles. This is due to the higher velocity coefficient for the VANES nozzles. It can be clearly seen that adding sealing flow in the system model significantly reduces the pre-swirl performance (ΔT_{dim} reducing by about 20%) with both the nozzles. The sealing flow provided was 14.8 % of the main pre-swirl flow with 50% swirl velocity of the rotor speed and at 30 K higher temperature than the main pre-swirl flow.

Figure 7 also shows calculated temperature differences using different numbers of nozzles. The change in the number of nozzles does not significantly affect the cooling air delivery temperature for the tested operating conditions. ΔT_{dim} changes less than 1.5 % for the AD nozzle and less than 4 % for VANES nozzle compare to original nozzle numbers.

5 TEMPERATURE LOSS CALCULATION

To separate temperature losses due to the nozzle, stator wall drag and sealing flow, Chew et al.'s [10] simple drag model is used, including sealing flow and accounting for some radial variation. For fully mixed free vortex conditions inside the pre-swirl chamber the following expressions can be derived from mass, angular momentum and energy balances.

Mass:
$$\dot{m}_{mix} = \dot{m}_p + \dot{m}_s \tag{5}$$

Angular moment:
$$\dot{m}_p r_p v_{\phi,p} + \dot{m}_s r_s v_{\phi,s} - \dot{m}_{mix} r_h v_{\phi,mix} = M + D \tag{6}$$

Energy:
$$\dot{m}_{mix} C_p T_{mix} - \left(\dot{m}_p C_p T_{in} + \dot{m}_s C_p T_s\right) = Q - M\Omega \tag{7}$$

where, $\dot{m}_p$, $\dot{m}_s$ and $\dot{m}_{mix}$ are main pre-swirl, sealing and mixed flow mass flow rates. $v_{\phi,s}$ and $v_{\phi,mix}$ are sealing and mixed flow swirl velocities. T_{in}, T_s and T_{mix} are main pre-swirl, sealing and mixed flow absolute total temperatures. Q denotes heat transfer to the cooling air from the walls. M and D are stator and rotor wall moment in the pre-swirl chamber, which may be estimated the same way as by Chew et al. [5] by the following expressions.

$$M = 0.5 A_{rotor} c_{rotor} r_{rotor} \rho \left|\Omega r - v_{\phi,mix}\right| \left(\Omega r - v_{\phi,mix}\right) \tag{8}$$

$$D = 0.5 A_{statot} c_{stator} r_{stator} \rho v_{\phi,mix}^2 \tag{9}$$

The friction factor for the stator walls has been estimated by $c_{stator} = 0.0534\, Re_\phi^{-0.2}$ and for the rotor walls by $c_{rotor} = 0.235\, Re_\phi^{-0.2}$ [5].

It is assumed that the leakage flow at the outer seal has the same relative total temperature as the pre-swirl cooling air delivery temperature, $T_{rel,h}$. Fully mixed absolute total temperatures, T_{mix} and $T_{rel,h}$ are related as follows.

$$T_{rel,h} = T_{mix} - \frac{v_{\phi,mix}^2 - \left(v_{\phi,mix} - \Omega r_h\right)^2}{2C_p} \tag{10}$$

Combining and rearranging equations (2), (5), (6), (7) and (10) gives the following expression for calculation of the individual losses in the pre-swirl chamber.

$$\underbrace{\frac{C_p\left(T_{in} - T_{rel,h}\right)}{0.5\Omega^2 r_h^2}}_{Actual\,temp.drop} = \underbrace{2\left(\frac{r_p}{r_h}\right)^2 \frac{v_{\phi,isen,p}}{\Omega r_p} - 1}_{Ideal\,temp.drop} - \underbrace{2(1-\eta)\left(\frac{r_p}{r_h}\right)^2 \frac{v_{\phi,isen,p}}{\Omega r_p}}_{nozzle\,loss}$$
$$- \underbrace{\frac{D}{0.5\dot{m}_p \Omega r_h^2}}_{stator\,wall\,drag\,loss} - \underbrace{\frac{Q}{0.5\dot{m}_p \Omega^2 r_h^2}}_{heat\,transfer\,loss} - \underbrace{\frac{\dot{m}_s}{\dot{m}_p}\left(\frac{C_p\left(T_s - T_{rel,h}\right)}{0.5\Omega^2 r_h^2} - 2\left(\frac{r_s}{r_h}\right)^2 \frac{v_{\phi,s}}{\Omega r_s} + 1\right)}_{sealing\,flow\,loss} \tag{11}$$

Equation (11) is similar to that of Chew et al. [5] with additional terms accounting for radius changes, sealing flow and heat transfer losses. Considering adiabatic conditions, (Q =

0), temperature drop and losses as percentage of the "ideal temperature drop" are shown in Figure 8. Results are shown from the CFD models for VANES and AD nozzles, and for the elementary model with η = 0.96. In the CFD calculations, losses due to sealing flow (including leakage at the outer seal) and incomplete mixing inside the chamber losses are combined and estimated as follows,

Sealing flow loss = Ideal temp drop – calculated temp drop - nozzle loss - stator wall drag loss

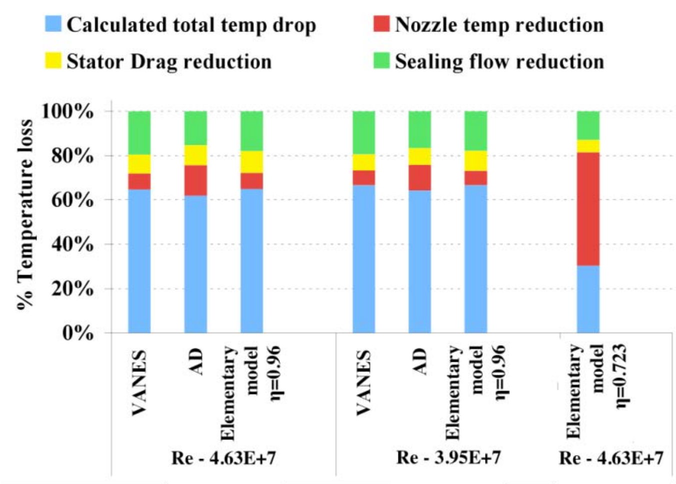

Figure 8: Temperature losses

In Figure 8, two sets of CFD results are shown for Re_ϕ= 4.63×10^7 and 3.95×10^7 but with the same C_w= 6.28×10^7 and $\dot{m}_s / \dot{m}_p = 0.148$. The elementary model estimates are shown for the same η value as calculated for the VANES nozzle. The elementary model estimate of the individual loss components agrees reasonably well with the CFD calculation. Again it can be seen that the VANES nozzles perform slightly better than the AD nozzles. The sealing flow loss contribution is significantly larger than other losses. As an example of a poor nozzle performance, results from the elementary model with η = 0.723 (equivalent to SD nozzle), are also shown in Figure 9. The poor nozzle design gives a large loss (~ 51%) in the full pre-swirl system. Clearly, aerodynamic design of the nozzle improves the pre-swirl performance significantly.

While the results in Figure 8 show good agreement between the CFD and elementary models, it should be noted that the elementary model is limited by assumptions of complete mixing in the pre-swirl chamber, the need to specify wall drag coefficients, heat transfer and nozzle characteristics. CFD can be used to accurate investigate these effects. Both methods are potential useful in industrial analysis and design.

6 CONCLUSIONS

Three different pre-swirl nozzle designs have been compared using CFD analysis of stand-alone and system analysis at engine operating conditions. Performances of the nozzles were assessed from the prediction of discharge coefficient, velocity coefficient and cooling air delivery temperature.

Two different turbulence models, k-ε and Spalart-Allmaras were tested, but both models gave similar results for the stand-alone nozzle discharge behaviour (C_D and η). Hence the k-ε turbulence model was used for further analysis. It has been observed that different numbers of nozzles and the presence of the rotor disc do not significantly affect the nozzle discharge behaviour. This conclusion is consistent with the previous experimental studies. The simple straight drilled nozzle showed significantly worse performance than the aerodynamically designed drilled and cascade vane nozzles with C_D and η being about 20 % lower. Overall performance of the cascade vanes was slightly better than the aerodynamically designed drilled nozzles. But the final choice may be dependent on other component design and nozzle manufacturing costs.

An elementary model was used to separate the different thermodynamic losses in the pre-swirl system including sealing flow. The drag model estimate of the losses agreed reasonably well with the CFD calculations. The temperature drop loss due to sealing flow was similar magnitude or larger than the pre-swirl chamber drag and nozzle combined losses for a range of tested operating conditions.

ACKNOWLEDGMENTS

The authors are grateful to the EPSRC and Rolls-Royce for financial support of this work, and to colleagues for helpful comments. Particular thanks are extended to Dr Colin Young at Rolls-Royce, Derby. The authors gratefully acknowledge the permission of Rolls-Royce plc to publish this paper.

REFERENCES

[1] Meierhofer, B., and Franklin, C. J., 1981. "An investigation of a preswirled cooling airflow to a turbine disc by measuring the air temperature in the rotating channels". *ASME Paper 81-GT-132.*

[2] El-Oun, Z. B., and Owen, J. M., 1989. "Preswirl blade-cooling effectiveness in an adiabatic rotor-stator system". *Journal of Turbomachinery,* **111**(4), pp. 522–529.

[3] Wilson, M., Pilbrow, R., and Owen, J. M., 1997. "Flow and heat transfer in a pre-swirl rotor-stator system". *Journal of turbomachinery,* **119**, pp. 364–373.

[4] Karabay, H., Wilson, M., and Owen, J. M., 2001. "Predictions of effect of swirl on flow and heat transfer in a rotating cavity". *International Journal of Heat and Fluid Flow,* **22**, pp. 143–155.

[5] Chew, J. W., Ciampoli, F., Hills, N. J., and Scanlon, T., 2005. "Pre-swirled cooling air delivery system performance". *ASME Paper GT2005-68323*.

[6] Lewis, P., Wilson, M., Lock, G., and Owen, J. M., 2007. "Physical interpretation of flow and heat transfer in

preswirl systems”. *Journal of Engineering for Gas Turbines and Power,* **129**, pp. 769–777.

[7] Benim, A. C., Cagan, M., Bricaud, C., Bonhoff, B., and Brillert, D., 2005. “Computational analysis of flow and heat transfer in direct-transfer pre-swirl systems for gas turbine cooling”. *6th European Conference on Turbomachinery, Lille, France*.

[8] Lock, G. D., Yan, Y., Newton, P. J., Wilson, M., and Owen, J. M., 2005. “Heat transfer measurements using liquid crystals in a preswirl rotating-disk system”. *Journal of Engineering for Gas Turbines and Power,* **127**, pp. 375–382.

[9] Javiya, U., Chew, J. W., Hills, N. J., Lock, G. D., Wilson, M., and Zhou, L., 2010. “CFD analysis of flow and heat transfer in a direct transfer pre-swirl system”. *ASME Paper GT2010-22964*.

[10] Chew, J. W., Hills, N. J., Khalatov, S., Scanlon, T., and Turner, A. B., 2003. “Measurement and analysis of flow in a pre-swirled cooling air delivery system”.*ASME Paper GT2003-38084*.

[11] Bricaud, C., Geis, T., Dullenkopf, K., and Bauer, H.-J., 2007. “Measurement and analysis of aerodynamic and thermodynamic losses in pre-swirl system arrangements”. *ASME Paper GT2007-27191*.

[12] Dittmann, M., Geis, T., Schramm, V., Kim, S., and Wittig, S., 2002. “Discharge coefficients of a preswirl system in secondary air systems”. *Journal of Turbomachinery,* **124**, pp. 119–124.

[13] Ciampoli, F., Chew, J. W., Shahpar, S., and Willocq, E., 2007. “Automatic optimization of preswirl nozzle design”. *Journal of Engineering for Gas Turbines and Power,* **129**, pp. 387–393.

[14] Hay, N., and Lampard, D., 1998. “Discharge coefficient of turbine cooling holes: A review”. *Journal of Turbomachinery,* **120**, pp. 314–319.

[15] McGreehan, W. F., and Schotsch, M. J., 1987. “Flow characteristics of long orifices with rotation and corner radiusing”. *ASME Paper 87-GT-162*.

[16] Snowsil, G. D., and Young, C., 2008. “Application of CFD to assess the performance of novel pre-swirl configuration”. *ASME Paper GT2008-50684*.

[17] Moinier, P., and Giles, M., 1998. “Preconditioned Euler and Navier-Stokes calculations on unstructured grids”. *6th ICFD Conference on Numerical Methods for Fluid Dynamics, Oxford, UK*.

[18] Lapworth, L., 2004. “Hydra-CFD: a framework for collaborative CFD development”. *International Conference on Scientific and Engineering Computation (IC-SEC)*.

[19] Martinelli, L., 1987. “Calculations of viscous flows with a multigrid methods”. *Ph.D Thesis, Dept. of Mech. and Aerospace Eng., Princeton University, USA*.

[20] Moinier, P., Muller, J.-D., and Giles, M. B., 2002. “Edge-based multigrid and preconditioning for hybrid grids”. *AIAA Journal,* **40**(10), pp. 1954–1960.

[21] Hills, N., 2007. “Achieving high parallel performance for an unstructured unsteady turbomachinery CFD code”. *The aeronautical journal,* **111**(1117), pp. 185–193.

[22] Spalart, P. R., and Allmaras, S. R., 1994. “One-equation turbulence model for aerodynamic flows”. *La Recherche Aerospatiale,* **1**, pp. 5–21.

